The centimeter-wavelength opacity of ammonia under deep jovian conditions

Kiruthika Devaraj [a,b,*], Paul G. Steffes [a], Danny Duong [a,c]

[a] School of Electrical and Computer Engineering, Georgia Institute of Technology, 777 Atlantic Drive NW, Atlanta, GA 30332-0250, United States
[b] Kavli Institute of Particle Astrophysics and Cosmology, Varian Physics #356, 382 Via Pueblo Mall, Stanford, CA 94305-4060, United States
[c] MPR Associates Inc., Alexandria, VA, 22314, United States

ABSTRACT

Extensive measurements of the centimeter-wavelength opacity of ammonia have been conducted under simulated deep jovian conditions using an ultra-high-pressure measurement system built at Georgia Tech. Over 1000 measurements of the opacity of ammonia have been conducted in the 5–20 cm wavelength range under simulated jovian conditions (pressures ranging from 0.05 to 99 bars, temperatures from 330 to 500 K) in a hydrogen–helium atmosphere. These and previous measurements conducted by Hanley et al. (Hanley et al. [2009]. Icarus, 202, 316–355) and Devaraj et al. (Devaraj et al. [2011]. Icarus, 212, 224–235) have been used to empirically derive a consistent ammonia opacity model for the 2 mm–20 cm wavelength range under the pressure and temperature conditions characteristic of the middle and deep jovian atmosphere. This model can be used reliably in the millimeter-wavelength range up to 3 bars of pressure and temperatures up to 300 K and in the centimeter-wavelength range up to 100 bars of pressure and temperatures up to 500 K. In addition, over 800 measurements of the 5–20 cm wavelength opacity of ammonia pressure-broadened by water vapor, hydrogen and helium have been conducted under simulated deep jovian conditions for the first time to study the influence of water vapor on the ammonia absorption spectrum. Based on these measurements, a new model has been developed. These laboratory data and the model show that water vapor has a measurable effect on the opacity of ammonia under jovian conditions. The laboratory study and the models will help to improve our understanding of centimeter-wavelength absorption by ammonia in the jovian planets in general, and specifically, will improve retrievals of ammonia and water vapor from the Juno microwave radiometer (MWR) at Jupiter.

© 2014 Elsevier Inc. All rights reserved.

1. Introduction

The microwave emission spectrum (centimeter- and millimeter-wavelengths) of Jupiter consists of thermal and non-thermal components: the thermal emission arises from the atmosphere and the non-thermal component (synchrotron emission), arises from the relativistic electrons and ions trapped in the inner radiation belts. Ground-based observations of Jupiter are dominated by thermal emission at frequencies greater than 3 GHz and non-thermal emission at frequencies less than 3 GHz (Berge and Gulkis, 1976). However, even at 10 GHz, there is a ∼10% contribution from the synchrotron component to the total emission from Jupiter

(Berge and Gulkis, 1976). Hence, the NASA mission Juno was launched in August 2011, to go into a highly elliptical polar orbit around Jupiter to avoid the synchrotron radiation (Matousek, 2005). Each elliptical 11-day polar orbit has an apojove of 39 Jupiter radii and a perijove of 1.06 Jupiter radii bringing the spacecraft between the radiation belt and the atmosphere (∼4500 km above the cloud tops). The primary science portion takes place when the spacecraft is positioned at perijove ±3–4 h, thereby avoiding the harsh synchrotron radiation. Juno will enter into orbit around Jupiter in August 2016. From the highly elliptical polar vantage point, the microwave radiometer (MWR) onboard Juno will measure the thermal emission from the atmosphere of Jupiter in the 1.3–50 cm range using six separate channels (Pingree et al., 2008). One of the primary goals of the Juno MWR is to measure the abundance of water and ammonia in Jupiter's atmosphere in order to aid the studies of our planetary system's formation and evolution. The thermal emission arises because of the presence of microwave-absorbing constituents such as ammonia and water

* Corresponding author at: Kavli Institute of Particle Astrophysics and Cosmology, Varian Physics #356, 382 Via Pueblo Mall, Stanford, CA 94305-4060, USA. Fax: +1 650 723 4840.
  E-mail addresses: kdevaraj@stanford.edu (K. Devaraj), steffes@gatech.edu (P.G. Steffes), dduong16@gmail.edu (D. Duong).

vapor and is dependent on the composition of the atmosphere, the observation frequency, and the temperature and pressure of the atmosphere (see, e.g. Janssen, 1993). To interpret the observed emission spectra of the jovian atmospheres, the emission spectra are compared with appropriate jovian atmospheric models, and the atmospheric composition and distribution of various constituents are obtained. A lack of laboratory measurements of the centimeter- and millimeter-wavelength properties of various gases has been cited as a major hindrance for modeling the atmospheres of the jovian planets (de Pater and Mitchell, 1993; de Pater et al., 2005).

The atmosphere of Jupiter and the other jovian planets (Saturn, Uranus, and Neptune), is primarily composed of hydrogen (H_2) and helium (He), with trace amounts of other constituents, such as methane (CH_4), water vapor (H_2O), ammonia (NH_3), hydrogen sulfide (H_2S), and phosphine (PH_3) (de Pater and Lissauer, 2001; Atreya et al., 2003). Gaseous ammonia contributes to strong absorption in the centimeter-wavelengths at Jupiter. Hence, accurate laboratory measurements of the centimeter-wavelength opacity of ammonia will facilitate retrievals of the concentration and distribution of ammonia as well as water vapor in Jupiter by the Juno MWR. The laboratory measurements of ammonia can also be used for interpreting ground-based and spacecraft-based observations of the centimeter-wavelength emission from the other jovian planets.

While a number of laboratory measurements of the opacity of ammonia under simulated jovian conditions have been conducted (see, e.g. Morris and Parsons, 1970; Steffes and Jenkins, 1987; Spilker, 1990), these measurements were made at limited wavelength-, pressure-, and temperature-range, and had large uncertainties associated with them. Hence, the models developed based on these measurements (e.g. Berge and Gulkis, 1976; Spilker, 1990; Joiner and Steffes, 1991) had limited accuracy. Recently, a rigorous laboratory measurement campaign was undertaken at Georgia Tech to study the microwave properties of ammonia under simulated jovian conditions. Laboratory measurements of the 1.3–20 cm-wavelength opacity of ammonia at pressures up to 12 bars were conducted by Hanley et al. (2009) under simulated jovian middle tropospheric conditions. Based on those measurements and millimeter-wavelength measurements conducted by Devaraj et al. (2011), a consistent ammonia opacity model was developed (Devaraj et al., 2011). This model can be used at pressures up to 12 bars in the centimeter-wavelength region and pressures up to 3 bars in the millimeter-wavelength region. However, this model cannot be applied to the deep atmosphere of Jupiter where the pressure exceeds a hundred bars.

In order to study the deep troposphere of the jovian planets, an ultra-high-pressure laboratory measurement system was designed and built at Georgia Tech (Karpowicz and Steffes, 2011b). Over 1000 measurements of the 5–20 cm opacity of ammonia broadened by hydrogen and helium at pressures up to 100 bars and temperatures up to 500 K have been conducted as part of this work. Based on these new measurements and the previous measurements conducted by Hanley et al. (2009) and Devaraj et al. (2011), a consistent absorption formalism has been developed to accurately characterize the opacity of ammonia in the centimeter-wavelength range at pressures up to 100 bars and temperatures up to 500 K, and millimeter-wavelength range at pressures up to 3 bars and temperatures up to 300 K. In addition, for the first time, the influence of water vapor on the ammonia absorption spectrum in the centimeter-wavelength region has been studied in the laboratory using the ultra-high-pressure measurement system. Over 900 laboratory measurements of the 5–20 cm wavelength opacity of ammonia broadened by water vapor under jovian atmospheric conditions have been made to investigate the role of water vapor in broadening the ammonia

absorption spectrum. (Laboratory measurements of the intrinsic opacity of water vapor in the 5–20 cm wavelength range in a hydrogen–helium atmosphere were conducted and an accurate model that can be used under jovian atmospheric conditions was developed by Karpowicz and Steffes (2011b).) The new ammonia–water vapor measurements made as part of this work have been used to empirically estimate the broadening coefficients of ammonia in the presence of water vapor, and a model has been developed for the centimeter-wavelength opacity of ammonia broadened by water vapor in a hydrogen–helium atmosphere at temperatures up to 500 K and pressures up to 100 bars.

The paper is organized as follows: a brief discussion of the measurement system and procedure is presented in Section 2. The ammonia–hydrogen–helium measurements, data fitting procedure, a new opacity model for ammonia pressure-broadened by hydrogen and helium at pressures up to 100 bars and temperatures up to 500 K, and the model evaluation is presented in Section 3. The measurements of ammonia in a water vapor–hydrogen–helium atmosphere, data fitting procedure, and a new model for the opacity of ammonia pressure-broadened by water vapor in addition to hydrogen and helium is presented in Section 4. Section 5 provides some discussions and conclusions.

2. Measurement system and procedure

The introduction of a lossy gas to a resonator reduces its quality factor (Q) and this property is used to measure its absorptivity (see, e.g. Bleaney and Penrose, 1947; Bleaney and Loubser, 1950). In addition, there is a shift in the center frequency of the resonances, and this property is used to measure the refractivity of the gas. The measurement theory is described in detail by DeBoer and Steffes (1994), Hanley and Steffes (2007) and Devaraj et al. (2011).

2.1. Measurement system

Karpowicz and Steffes (2011b) built an ultra-high-pressure measurement system to conduct measurements of the opacity of water vapor in the presence of hydrogen and helium in the 5–20 cm-wavelength range at pressures up to 100 bars and temperatures up to 500 K. This system was modified to enable measurements of ammonia and ammonia–water vapor in a hydrogen helium atmosphere under the same pressure and temperature conditions for the work described in this article. This system consists of a jovian atmospheric simulator, centimeter-wavelength subsystem, and a data-handling subsystem. A brief description of each of these subsystems is provided below, and a detailed description is provided by Karpowicz and Steffes (2011b).

2.1.1. Jovian atmospheric simulator

The jovian atmospheric simulator consists of an ultra-high pressure vessel, designed by Karpowicz and Steffes (2011b) and custom built by Hays Fabrication and Welding. The pressure vessel that can accommodate up to 100 bars of pressure and 560 K temperature is placed in a Grieve® industrial oven (model AB-650 rated to 615 K). The oven acts as a stable temperature chamber and maintains the temperature within ±0.1 °C. The oven is placed on an outdoor concrete pad and enclosed by a metallic shed for protection.

A 304 stainless steel pipe filled with distilled, deionized water is placed inside the oven and connected to the pressure-vessel to produce water vapor. Ultra-high-purity UHP300 grade Airgas® gas bottles (hydrogen, helium, ammonia, pre-mixed hydrogen/helium, and argon) required for the measurements are placed on a gas cylinder rack adjacent to the shed. A gas delivery pressure

regulator, Matheson® model 3030-580 is used for argon and helium, Matheson® model 3030-350 is used for hydrogen, and Airgas® model Y11E444B660 is for ammonia. A Teledyne-Hastings® HFM-I-401 industrial flow meter rated to 103 bars pressure is used for mass flow sensing. Swagelok® fittings and seamless stainless steel 3/8″ outer diameter (OD) tubing are used to connect the components in the gas handling subsystem. An exhaust valve is used to vent the gases to ambient pressure, and a Welch DuoSeal® vacuum pump model 1376B-01 is used to evacuate the pressure vessel from ambient pressure down to vacuum (better than 0.1 mbar).

A GE Druck DPI 10430A Digital Test Gauge is used for pressure sensing in the 0 to 2 bar range, and a GE Druck DPI 104300A Digital Test Gauge is used for pressure sensing in the 2 to 20 bar range. An Omega® PX1009L0-1.5KAV pressure transducer connected to a HP 34401A multimeter is used for sensing pressures up to 100 bars. An Omega® resistance temperature detector RTD (PR-11-2-100-1/4-9-E) is used for sensing gas temperature in the pressure vessel. A high-temperature thermometer/hydrometer assembly E+E Elektronik® EE33-MFTI9205HA07D05/AB6-T52 was used for temperature sensing the initial set of measurements conducted below 450 K. T-type thermocouple probes are used for temperature sensing at various points inside and outside the oven. A block diagram of the various components of the simulator is shown in Fig. 1.

2.1.2. Centimeter-wavelength subsystem

Over the past twenty years, the centimeter-wavelength subsystem has been continuously improved (see, e.g. DeBoer and Steffes, 1996; Hanley and Steffes, 2007; Karpowicz and Steffes, 2011b). A type 304 stainless steel cylindrical cavity resonator with gold-plated interior is placed inside the ultra-high pressure vessel. The interior of the cavity resonator measures approximately 13.1 cm in diameter and 25.5 cm in height, and it is ideal for measurements

in the 5–20 cm wavelength range. One dozen high-Q, low-asymmetry resonances were selected and used as "standard resonances" for all the measurements. A detailed description of the selection criteria for the resonances was provided by Hanley et al. (2009).

Ceramtec® microwave feedthroughs model 16545-01-CF are used for coupling microwave energy to the resonator via Times Microwave® SiO_2 cables through the top-plate of the pressure-vessel. The SiO_2 cables are rated to 875 K and the Ceramtec feedthroughs are rated to 103 bars and 625 K. Exterior to the pressure vessel, two 1 m long sections of high-temperature Times Microwave® M17/86-00001 (RG-225) cables fitted with type-N connectors are connected to the Ceramtec feedthroughs via high-temperature type-N to SMA adapters. The other end of these RG-225 cables with type-N bulkheads are positioned outside of the oven via holes that were drilled on the side wall of the oven. Two sections of ~24.4 m length Andrews® CNT 600 microwave cables, rated to 350 K, are connected to the type-N bulkheads on the RG-225 cable assemblies outside the oven and connect to an Agilent® E5071C vector network analyzer that is placed inside the laboratory environment to ensure its temperature stability. The network analyzer S-parameter measurements are recorded by the data acquisition system via General Purpose Interface Bus (GPIB or IEEE-488).

2.1.3. Data acquisition system

The data acquisition subsystem consists of (i) a laptop computer connected to the network analyzer and multimeter via a GPIB and National Instruments NI-488.2 interface card, and (ii) a data logging computer connected to the various pressure and temperature sensors via extended USB buses and USB to RS-232 adapters. The extended USB buses allow the data logging computer to remain
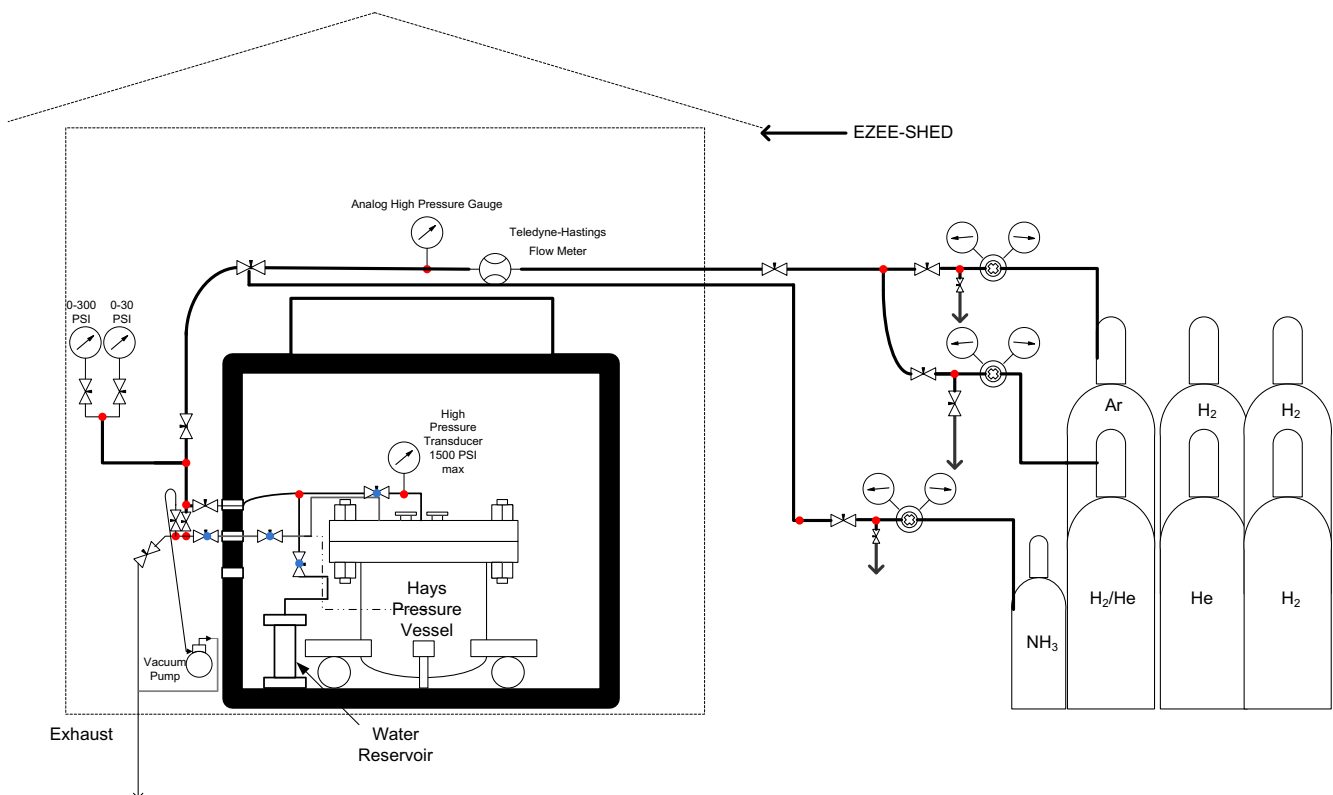

Fig. 1. The Georgia Tech jovian atmospheric simulator is used for studying the centimeter-wavelength properties of ammonia under simulated jovian conditions (Karpowicz and Steffes, 2011b). The high temperature valves inside and close to the oven are shown with a blue dot. (For interpretation of the references to color in this figure legend, the reader is referred to the web version of this article.)

inside the laboratory. The network analyzer is controlled via Matlab® software and the Standard Commands for Programmable Instruments (SCPI) and the suite of pressure and temperature sensors are controlled via Python®. The Matlab software used is similar to that used by Hanley and Steffes (2007) and a detailed description of the data acquisition system is provided by Karpowicz (2010).

2.2. Procedure

The measurement procedure consists of the following steps:

Vacuum 1: The pressure vessel is evacuated with a vacuum pump until a vacuum lower than 0.1 mbar is reached. The valves next to the oven wall are closed and the vacuum pump is shut-off while measurements are taken in order to prevent the pump vibrations from disturbing the measurement set-up in general and the microwave cables in particular. "Standard resonances" selected based on the criteria discussed by Hanley and Steffes (2007) are measured at vacuum.
Test gases: Lossy test gases such as ammonia, water vapor, hydrogen, and helium are added to the system, allowed to stabilize for 8–10 h, and then the frequency shifted resonances are measured at different pressures. More description of the test gas measurements is provided in Section 3.
Vacuum 2: The pressure vessel is evacuated for at least 12 h to remove the test gases and the resonances are measured again at vacuum.
Dielectric matching: A lossless gas such as argon is added to the system to shift the center frequency of the resonances by the same amount as the test gases to remove the effects of dielectric loading (see, e.g. Spilker, 1990), and the resonances are measured.
Vacuum 3: The pressure vessel is evacuated for at least 12 h, and the resonances are measured once again at vacuum.
Signal level: It is important to account for the losses in the long microwave cables and the many connectors between the network analyzer and the cavity resonator to correct the measurements of the transmissivities of the test gases and the dielectric matching gas. Three sets of straight-through measurements of signal levels are made (without the resonator present) under the same temperature conditions at each pressure/frequency point of the test gases. These measurements are used to correct the measurements of transmissivities of the test gases and lossless gases present in the resonator for losses in the microwave cables and connectors. These measurements involve disconnecting the RG-225 cables from the Ceramtec feedthroughs and connecting the cables together via a high-temperature female-to-female SMA adapter and making multiple measurements (about 30) at the standard resonant frequencies. Between the signal level measurements, all the coax connections are remade in order to better statistically characterize their reproducibility. These measurements are only made at the end of each measurement cycle so that the system's temperature stability is not affected during the measurement cycle, since they involve opening the temperature chamber multiple times to reconnect the coax assemblies, which might temporarily alter the temperature of the chamber.

2.3. Data processing

Data processing is performed after each measurement cycle is completed using software written in Matlab®. The software used is similar to that described by Hanley and Steffes (2007), but with modifications to account for the configuration of the new measurement system. The software reads the raw data files, runs smoothing and processing algorithms, and calculates the absorptivity of the test gas at each measurement frequency, pressure, temperature, and concentration (fTPC). The cable losses at each measurement fTPC point are calculated by taking the mean of 30 sweeps per set of the signal level measurements, and then averaging the three sets of the signal level measurements. The test gas insertion loss and dielectrically matched insertion loss are obtained by subtracting the cable losses from the peak power measurements of the test gases and the dielectrically matched gas, respectively. The uncertainties associated with the measurements are: (i) instrumental errors (σ_n), (ii) errors in dielectric matching (σ_{diel}), (iii) transmissivity or signal-level errors (σ_{trans}), (iv) errors due to asymmetry in resonances (σ_{asym}), and (v) errors in measurement conditions (σ_{cond}) due to uncertainties in measurement temperature, pressure, and concentration (see, e.g. Hanley and Steffes, 2007; Karpowicz and Steffes, 2011b). Although σ_{cond} does not directly affect the measurements, it still needs to be accounted for while creating accurate models for opacity based on experimental data, and is computed as

$$\sigma_{cond} = \sqrt{\sigma_{temp}^2 + \sigma_p^2 + \sigma_c^2}, \tag{1}$$

with σ_{temp}, σ_p, and σ_c representing the 2σ uncertainties in opacity corresponding to the uncertainties in temperature, pressure, and concentration, respectively. Each of these uncertainties is calculated by halving the difference between the maximum modeled opacity and the minimum modeled opacity, with each measurement uncertainty. Since the dependence of σ_{cond} on the opacity is not known while making the measurements, this uncertainty is maintained separately from σ_{tot}. σ_{cond} appears as a spread in the modeled opacity, given the uncertainty in the conditions, and this uncertainty is negligible compared to σ_{tot}. The 95% confidence σ_{tot} for the opacity measurements is calculated as per Hanley et al. (2009).

$$\sigma_{tot} = \sqrt{\sigma_n^2 + \sigma_{diel}^2 + \sigma_{trans}^2 + \sigma_{asym}^2}. \tag{2}$$

The predominant uncertainties in the measurements described in this article arise from errors in transmissivity and the asymmetric nature of the resonances. Fig. 2 shows the percentage median contribution of the different measurement uncertainties to the total uncertainty.

2.4. Compressibility

The thermodynamic pure fluid properties used in this work were obtained from the REFPROP database of the National Institute
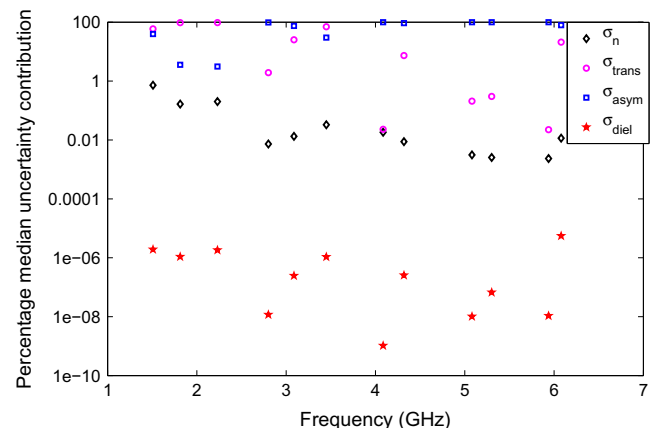

Fig. 2. Percentage median contribution of the different measurement uncertainties to the total uncertainty.

of Standards and Technology (NIST) (Lemmon et al., 2007) and subroutines were written in Matlab to access the database. In the ultra-high-pressure realm (characteristic of the very deep interiors of the jovian atmospheres), the non-ideal nature of fluid mixtures should also be included since Dalton's law of partial pressures breaks down (Span, 2000). In this work, the latest equations of state for pure fluids and mixtures, where available, have been employed to compute their thermodynamic properties at pressures up to 100 bar. Detailed description of the equations of state for hydrogen, helium, ammonia, and water vapor are provided by Devaraj (2011) and the equations of state for the hydrogen, helium, methane, and water vapor mixture is provided by Karpowicz and Steffes (2013).

3. Ammonia opacity measurements

The measurement process involved an extensive series of measurements of the opacity of ammonia under simulated deep jovian conditions at pressures up to 100 bars and temperatures up to 500 K. A total of 1176 measurements of the 5–20 cm-wavelength absorptivity of pure ammonia and ammonia broadened by hydrogen and/or helium have been made using the high-pressure centimeter-wavelength measurement system. Each measurement sequence first involved the addition of gaseous ammonia to an evacuated chamber up to the desired pressure, and pure ammonia measurements were made to accurately characterize its self-broadening parameters. In this work, pure ammonia measurements were made in the 0.046–0.133 bar pressure range. Gaseous helium was then added to the system up to the desired pressure and ammonia–helium mixture measurements were made to characterize the helium-broadening parameters. The ammonia–helium mixture measurements were made in the 7–20 bar pressure range. Gaseous hydrogen was then added to the pressure vessel, in 10–20 bar pressure increments, and the ammonia–helium–hydrogen mixture measurements were made at pressures up to 100 bar. A few measurements of the ammonia–hydrogen mixture opacity at pressures up to 100 bars were also made to accurately characterize the hydrogen-broadening parameters. A total of 180 data points of the opacity of pure ammonia, 156 data points of the opacity of ammonia–helium mixture, 120 data points of the opacity of ammonia–hydrogen mixture, and 720 data points of the opacity of ammonia–helium–hydrogen mixture were measured, with each data point uniquely representing a combination of pressure, temperature, mixing ratio (concentration), and frequency. Table 1 lists the measurements taken along with the experiment dates. The pressure values provided in the table correspond to the measured maximum pressure readings of the pressure sensors. The

processed data are provided in the online Supplementary materials section (*NH3H2HeMeasurements.mat*).

3.1. Data fitting

One of the primary goals of this work has been to develop a consistent model, based on laboratory measurements, that can be used to estimate the opacity of ammonia in a hydrogen–helium atmosphere under diverse frequency/temperature/pressure/concentration (fTPC) conditions. The data fitting process is similar to that used by Devaraj et al. (2011). Ammonia opacity measurements in the 75–150 GHz at pressures up to 3 bars and temperatures up to 300 K made by Devaraj et al. (2011), the 1.5–27 GHz measurements at pressures up to 12 bars and temperatures from 184 K to 450 K made by Hanley et al. (2009), and the high-pressure measurements in the 1.5–6 GHz made as part of this work were utilized for the data fitting process. A data set consisting of 250 data points measured by Hanley et al. (2009) in the 22–40 GHz range using a Fabry–Perot resonator (FPR) at room temperature and pressures up to 3 bars was used as an independent test set to verify the validity of the model (see Table 8 for the goodness of fit of the model to the 22–40 GHz data), this data set was not used in the model development process. The Levenberg–Marquardt optimization technique (Levenberg, 1944; Marquardt, 1963) used in this work has a minimization function

$$\chi = \frac{\sqrt{DW} \times (\alpha_{measured} - \alpha_{model})}{\sigma_{measured}}, \tag{3}$$

where DW is the data weight assigned to the data point, $\alpha_{measured}$ is the measured opacity, α_{model} is the modeled opacity, and $\sigma_{measured}$ is measured uncertainty in opacity. The measured uncertainty in opacity is calculated as

$$\sigma_{measured} = \sigma_{tot} + \sigma_{cond}, \tag{4}$$

where σ_{tot} is the total measurement uncertainty and σ_{cond} is the uncertainty due to measurement conditions. Multiple iterations of the minimization function with random input starting values were run, to minimize the sum of squared value of χ and to arrive at a convergent solution. The data weight is given as (Hanley et al., 2009)

$$DW = \frac{1}{n_f} + \frac{1}{n_T} + \frac{1}{n_P} + \frac{1}{n_C}, \tag{5}$$

where n_f, n_T, n_P, and n_C represent the number of measurements conducted at each frequency, temperature, pressure, and gas concentration range, in the four-dimensional fTPC space. The data points are divided into roughly equally spaced fTPC bins and scaled

Table 1
Listing of all experiment sequences of the 5–20 cm-wavelength ammonia opacity measurements conducted using the high-pressure system as part of this work.

Experiment dates	Temperature (K)	Maximum pressure (bar)	NH₃ pressure (bar)	He pressure (bar)
09/2009	376.0	94.66	0.0899	12.53
09/2009	375.5	95.51	0.0798	13.63
10/2009	375.2	96.11	0.0580	14.0
10/2009	373.2	95.59	0.1096	11.92
11/2009	446.5	95.34	0.1	7.35
12/2009	446.8	93.54	0.0824	0
12/2009	446.6	94.01	0.0805	19.07
01/2010	322.6	92.66	0.0838	16.55
02/2010	332.9	91.73	0.0462	15.58
02/2010	401.0	96.17	0.0813	11.98
03/2010	452.1	97.6	0.133	12.42
09/2010	503.6	94.17	0.0850	16.64
10/2010	502.8	89.99	0.0662	9.40
11/2010	502.6	96.47	0.1046	0
11/2010	502.1	98.44	0.1248	10.75

with their data weights to prevent the model from being skewed toward the most frequently measured conditions. The data fitting process was done in two stages. In the first stage, the free parameters for the rotational and v_2 roto-vibrational transitions were estimated using a measurement database consisting of the 75–150 GHz measurements conducted by Devaraj et al. (2011) and the 1.5–27 GHz measurements conducted by Hanley et al. (2009). Nominal values of the free parameters for the inversion transitions were also obtained in this stage and later revised during the second stage of data fitting. In the second stage, the 1.5–6 GHz high-pressure measurements conducted as part of this work were added to the measurement database and the free parameters for the inversion transitions were estimated.

3.1.1. Optimization step 1: free parameters of the rotational and v_2 roto-vibrational transitions

In the first stage of data fitting, the 75–150 GHz measurements and the 1.5–27 GHz measurements were used to create the fTPC space. The breakdown of the fTPC space is listed in Table 2. The free parameters for pure ammonia were estimated first, followed by the parameters for hydrogen and helium. The dataset of pure ammonia measurements were divided into two subgroups: Group I (GI) with $v \leqslant 100$ GHz, and Group II (GII) with $v > 100$ GHz. GI was used for estimating the free parameters of the inversion and rotational transitions of ammonia since only these transitions contribute significantly to the opacity at $v \leqslant 100$ GHz. GII was used for estimating the free parameters of the v_2 roto-vibrational transitions since the first strong v_2 transition is at 140 GHz and these transitions contribute to the opacity at $v > 100$ GHz. After the ammonia free parameters were estimated, they were assigned to the subsequent optimization steps to estimate the free parameters for hydrogen and helium using the ammonia–hydrogen–helium mixture measurements. The mixture measurements were subdivided in a similar fashion to the ammonia measurements into two groups: Group III (GIII) with $v \leqslant 100$ GHz and Group IV (GIV) with $v > 100$ GHz. GIII was used for estimating the hydrogen and helium free parameters of the inversion and rotational transitions and GIV was used for estimating the hydrogen and helium free parameters for the v_2 roto-vibrational transitions. This procedure was repeated multiple times with random input seed values (generated using a Matlab pseudorandom generator function) for the free parameters, to ensure that convergence was achieved with random seed inputs. For neutral gases, the temperature coefficient is between 0.5 and 1.0 (Townes and Schawlow, 1955). Therefore, an upper limit of 1.0 and lower limit of 0.5 were enforced on the random numbers generated for the temperature coefficients. After this stage of optimization, the values for the free parameters of the rotational and v_2 roto-vibrational transitions were constrained. The values for the free parameters of the inversion transitions that were obtained after this stage of optimization were further revised during the second stage of optimization to develop a model that can be used under the high-pressure conditions characteristic of the deep jovian atmosphere.

3.1.2. Optimization step 2: free parameters of the inversion transitions

The values that were obtained for the inversion transitions of ammonia after the first optimization step can be used to estimate the centimeter-wavelength ammonia opacity under jovian conditions at pressures up to 12 bar (Devaraj et al., 2011). However, these values cannot be used under the deep jovian conditions because they were not optimized to perform under those conditions. It was possible to obtain a consistent formalism that performs well in both the low-pressure (pressures up to 15 bars) and the high-pressure (pressures greater than 15 bars and up to 100 bars) regimes, by using two sets of parameters for the inversion transitions and incorporating a pressure-dependent switch. The procedure used to estimate the pressure-dependent free parameters of the inversion transitions is discussed below.

The fTPC space for the second stage of data fitting includes the 1.5–6 GHz high-pressure measurements made as part of this work, in addition to the 1.5–27 GHz measurements conducted by Hanley et al. (2009), and the 75–150 GHz measurements (Devaraj et al., 2011). The breakdown in the fTPC space of the measurement database used in the second stage of optimization is listed in Table 3. In this stage of data fitting, only the free parameters of the inversion transitions were optimized. To best fit the measured data, two sets of parameters for the inversion transitions were derived, and a pressure-dependent switch was included in the model to ensure consistent results over the wide pressure range (0.01 bar to 100 bar) characteristic of the middle and deep troposphere of the jovian planets. This was, however, not required for the rotational and the v_2 roto-vibrational transitions of ammonia since these transitions occur at high frequencies (the first rotational transition of ammonia occurs at 572 GHz and the first strong v_2 inversion transition of ammonia occurs at 140.14 GHz) and the jovian atmospheric layers that contribute to the emission at these frequencies have pressures less than a few bar (upper and middle troposphere of the jovian planets). For example, the atmospheric layers of Jupiter that contribute to the emission at 140 GHz have pressures between 0.5 and 3 bar, whereas at 1 GHz, the contribution is from the atmospheric layers with pressures up to hundreds of bars (Karpowicz, 2010). Hence, it was sufficient to derive two sets of parameters, the low-pressure and high-pressure parameters, for the inversion transitions alone.

In the second stage of data fitting, the measurements were split into two groups: Group V (GV) consisting of data points with $P \leqslant 15$ bar and Group VI (GVI) consisting of the data points with $P > 15$ bar. The pure ammonia measurements were used to obtain the ammonia free parameters for the inversion transitions. Since the pure ammonia measurements were made under low-pressure conditions ($P < 0.8$ bar), only one set of parameters was estimated. The ammonia–helium mixture measurements with $P \leqslant 15$ bar (GV) were used to obtain the low-pressure helium-broadening parameters for the inversion transitions and the ammonia–helium mixture measurements with $P > 15$ bar (GVI) were used to obtain the high-pressure helium-broadening parameters for the inversion transitions. The ammonia–hydrogen mixture measurements with $P \leqslant 15$ bar (GV) were used to obtain the low-pressure

Table 2
The breakdown in the fTPC space of the measurement database consisting of the 75–150 GHz Fabry–Perot resonator (FPR) measurements (Devaraj et al., 2011) and the 1.5–27 GHz cavity resonator measurements (Hanley et al., 2009) used in the first stage of optimization.

Frequency range (GHz)	n_f	Temperature range (K)	n_T	Pressure range (bar)	n_P	Concentration range (%)	n_C
$f < 6$	874	$T < 210$	291	$P < 0.5$	459	$C < 0.5$	380
$6 \leqslant f < 27$	557	$210 \leqslant T < 230$	650	$0.5 \leqslant P < 1$	213	$0.5 \leqslant C < 1$	578
$75 \leqslant f < 100$	329	$230 \leqslant T < 300$	1195	$1 \leqslant P < 2$	533	$1 \leqslant C < 4$	481
$100 \leqslant f < 120$	393	$300 \leqslant T < 380$	112	$2 \leqslant P < 5$	761	$4 \leqslant C < 10$	557
$120 \leqslant f < 150$	291	$380 \leqslant T < 450$	196	$5 \leqslant P \leqslant 12.5$	478	$10 \leqslant C \leqslant 100$	448

Table 3

The breakdown in the fTPC space of the measurement database consisting of the 75–150 GHz FPR measurements (Devaraj et al., 2011), 1.5–27 GHz cavity resonator measurements (Hanley et al., 2009), and the 1.5–6 GHz high-pressure measurements (this work) used in the second stage of optimization.

Frequency range (GHz)	n_f	Temperature range (K)	n_T	Pressure range (bar)	n_P	Concentration range (%)	n_C
$f < 5$	1340	$T < 230$	941	$P < 1$	852	$C < 0.1$	208
$5 \leqslant f < 10$	847	$230 \leqslant T < 310$	1195	$1 \leqslant P < 3$	914	$0.1 \leqslant C < 0.5$	1000
$10 \leqslant f < 27$	420	$310 \leqslant T < 385$	592	$3 \leqslant P < 12$	867	$0.5 \leqslant C < 1$	710
$75 \leqslant f < 100$	329	$385 \leqslant T < 460$	592	$12 \leqslant P < 40$	363	$1 \leqslant C < 10$	1074
$100 \leqslant f < 150$	684	$460 \leqslant T < 510$	300	$40 \leqslant P \leqslant 100$	624	$10 \leqslant C \leqslant 100$	628

hydrogen-broadening parameters for the inversion transitions and the ammonia–hydrogen mixture measurements with $P > 15$ bar (GVI) were used to obtain the high-pressure hydrogen-broadening parameters for the inversion transitions. After this step, the low-pressure and high-pressure inversion transition parameters were further optimized and fine-tuned by using the ammonia–helium–hydrogen mixture measurements. This procedure was repeated several times with different input seed values for the free parameters, until convergent solutions were obtained.

3.2. New consistent ammonia absorption formalism

The laboratory measurements were used to develop a consistent mathematical formalism that can be used to estimate the opacity of ammonia under jovian atmospheric conditions. The formulations for the ammonia opacity model are described in detail by Devaraj et al. (2011), but they are provided here for completeness. The absorption of a collisionally broadened gas is given as

$$\alpha = \sum_j A_j \pi \Delta v_j F_j(v, v_{(0,j)}, \ldots) \quad (\text{cm}^{-1}), \tag{6}$$

where j represents the line index, A_j represents the absorption at the line center in cm^{-1}, Δv_j represents the half width at half max, or the linewidth, in cm^{-1}, $F_j(v, v_{0,j}, \ldots)$ represents the lineshape function in cm, $v_{(0,j)}$ represents the frequency at the line center in cm^{-1}, and v represents the frequency of the incident electromagnetic wave in cm^{-1} (see, e.g. Townes and Schawlow, 1955). The absorption at each line center is calculated using the line intensity information from the latest JPL catalog, version 5, updated on September 2010 (Yu et al., 2010a,b,c) as per Pickett et al. (1998)

$$A_j = \frac{n I_j(T)}{\pi \Delta v_j} \quad (\text{cm}^{-1}), \tag{7}$$

where n represents the number density of the gas in molecules/cm^3, $I_j(T)$ represents the intensity of the line in $\text{cm}^{-1}/(\text{molecule/cm}^2)$ at temperature T, and with Δv_j expressed in cm^{-1}. The references from which the latest JPL spectral line catalog entries were obtained are listed on the JPL website and are provided as Supplementary material to this paper (*d017002.pdf* and *d017004.pdf*). The number density n is calculated as

$$n = \frac{0.1 \times P_{ideal}}{k_B T}, \tag{8}$$

where P_{ideal} represents the ideal partial pressure of the gas under consideration in bar, T represents the temperature in K, and k_B represents Boltzmann's constant (1.38×10^{-23} J/K). The ideal partial pressure of a gas is computed from its density and temperature. In this work, the density of a gas is computed from its equation of state. The equations of state of pure gases, hydrogen, helium, ammonia, and water are given by Devaraj (2011) and Karpowicz and Steffes (2013), and the equation of state for the hydrogen–helium–water vapor mixture is given by Karpowicz and Steffes (2013). The thermodynamic properties of gases and mixtures were obtained from the NIST database (Lemmon et al., 2007). The ideal pressure (in bar) is computed as,

$$P_{ideal} = \rho \frac{R_0}{M} T, \tag{9}$$

where ρ represents the gas density in g/m^3, R_0 represents the ideal gas constant for the gas, M represents the molecular mass of the gas in g/mol and T represents the measured temperature in K. The value for R_0 used in this work is equal to $8.314472 \times 10^{-5} \left(\frac{\text{m}^3 \text{ bar}}{\text{Kmol}} \right)$ for all the gases except helium. For helium, the equation of state requires the use of the older value $8.31431 \times 10^{-5} \left(\frac{\text{m}^3 \text{ bar}}{\text{Kmol}} \right)$. The line intensity at the measurement temperature (T) is calculated as

$$I_j(T) \approx I_j(T_0) \left(\frac{T_0}{T} \right)^{\eta+1} \exp \left(\left(\frac{1}{T_0} - \frac{1}{T} \right) E_{(l,j)} (hc/k_B) \right), \tag{10}$$

where $I_j(T_0)$ represents the intensity of the line at the reference temperature T_0, $E_{(l,j)}$ represents the lower state energy of transition in cm^{-1}, c is the speed of light in cm/s, h is Planck's constant in J-sec, and η represents the temperature dependence and is $\approx 3/2$ for non-linear and symmetric-top molecules such as ammonia, and 1 for linear molecules. The values of $v_{(0,j)}$, $I_j(T_0)$, and $E_{(l,j)}$ at the reference temperature are taken from the latest JPL spectral line catalog (Pickett et al., 1998) (Version 5, September 2010). The values of $I_j(T_0)$ given in the JPL catalog have units of $\log_{10}(\text{nm}^2 \text{ MHz})$ and must be taken as the exponent of 10 and then divided by $2.99792458 \times 10^{18}$ to be converted to $\text{cm}^{-1}/(\text{molecule/cm}^2)$. The linewidth for a gas mixture is calculated by

$$\Delta v_j = \sum_i \Delta v_{(i,j)}^o P_{(i,ideal)} \left(\frac{T_0}{T} \right)^{\xi_{ij}} \quad (\text{cm}^{-1}), \tag{11}$$

where for the gas i and line j, $\Delta v_{(i,j)}^o$ represents the line broadening parameter in cm^{-1}/bar, $P_{(i,ideal)}$ represents the ideal partial pressure of the gas in bar (computed using Eq. (9)), and ξ_{ij} represents the temperature dependence of the line broadening parameter. The temperature dependence is calculated as (e.g., Townes and Schawlow, 1955)

$$\Delta v_j \propto T^{-(m+1)/2(m-1)} = T^{-\xi}, \tag{12}$$

where $1 \leqslant m < \infty$. For neutral gases, $m = 3$ is a lower limit and hence $0.5 < \xi < 1.0$.

3.2.1. Line parameters

The NH_3 and $NH_3 - v_2$ line parameters were obtained from the JPL spectral line catalogs (Pickett et al., 1998) (Version 5, September 2010). A modified Ben–Reuven lineshape (Ben-Reuven, 1966) was used for the inversion transitions, and a modified Gross lineshape (Gross, 1955) was used for the rotational and v_2 rotovibrational transitions in the new model. The self- and foreign-gas-broadening parameters were extracted from various sources, including laboratory measurements and calculations, where available. For the line transitions where no broadening parameters were available in the literature, they were made free parameters in the data fitting process and empirical values were derived for this work.

3.2.2. Ammonia opacity formalism

The cumulative ammonia opacity from the inversion, rotational, and roto-vibrational transitions is calculated by

$$\alpha = (\alpha_{inv} + \alpha_{rot} + \alpha_{v_2}) \times 434294.5 \quad (\text{dB/km}), \tag{13}$$

where α_{inv}, α_{rot}, and α_{v_2} are the opacities from the inversion, rotational, and v_2 transitions, respectively, in cm^{-1}. The factor 434294.5 converts the total absorptivity from cm^{-1} to dB/km.

A detailed description of the opacity calculations from the inversion, rotational, and roto-vibrational transitions is given by Devaraj et al. (2011) for a model that can operate at pressures up to 12 bars. The current work extends the model developed by Devaraj et al. (2011) by incorporating new cm-wavelength measurements of ammonia opacity in the presence of hydrogen and helium at pressures up to 100 bars in the data fitting process for the inversion transitions. The roto-vibrational and rotational transitions of ammonia occur in the millimeter-wavelength range, and the jovian atmospheric layers that contribute to emission at these frequencies have pressures less than a few bars (Karpowicz, 2010). Since the model constants derived for the roto-vibrational and rotational transitions by Devaraj et al. (2011) are applicable at these pressure ranges, these model constants were not altered in this work. Two sets of new model constants were obtained for the inversion transitions of ammonia by optimizing the free parameters. The low-pressure inversion transition model constants are applicable when $P \leqslant 15$ bars and the high-pressure inversion transition model constants are applicable when $P > 15$ bars. However, since the two sets of coefficients are not continuous, when using this ammonia model in a radiative transfer model to simulate the emission spectrum of the jovian planets, an interpolation of the two parameter sets should be used near the 15 bar pressure level to avoid the discontinuity in the emission spectrum. The formulations for the inversion, roto-vibrational, and rotational transitions are provided here for completeness even though these formulations have been provided by Devaraj et al. (2011). The inversion line opacity is given by

$$\alpha_{inv} = \frac{0.1 D_{inv} P_{NH_3}}{k_B T} \left(\frac{2}{\pi}\right) \left(\frac{T_0}{T}\right)^{\eta+1}$$
$$\times \sum_j \left(I_j(T_0) \exp \left(\left(\frac{1}{T_0} - \frac{1}{T} \right) E_{(l,j)} \left(\frac{hc}{k_B} \right) \right) \left(\frac{v}{v_{(0,j)}} \right)^2 \right.$$
$$\left. \left[\frac{(\gamma_j - \zeta_j)v^2 + (\gamma_j + \zeta_j) \left[(v_{(0,j)} + \delta_j)^2 + \gamma_j^2 - \zeta_j^2 \right]}{\left[v^2 - (v_{(0,j)} + \delta_j)^2 - \gamma_j^2 + \zeta_j^2 \right]^2 + 4v^2 \gamma_j^2} \right] \right) \quad (\text{cm}^{-1}), \tag{14}$$

where for the inversion line j, $v_{(0,j)}$, γ_j, ζ_j, and δ_j are the center frequency, linewidth, coupling parameter, and shift parameter, respectively, in cm^{-1}, and D_{inv} is a unitless scale factor. The frequency, linewidth, coupling, and shift parameters should be converted to cm^{-1} from GHz before they are used in the opacity equation. The linewidth and coupling parameters are calculated by summing the contributions from ammonia, hydrogen, and helium. The linewidth and coupling parameter are given by

$$\gamma_j = \gamma_{H_2} P_{H_2} \left(\frac{300}{T}\right)^{\Gamma_{H_2}} + \gamma_{He} P_{He} \left(\frac{300}{T}\right)^{\Gamma_{He}}$$
$$+ \gamma_{NH_3} \gamma_{(0,j)} P_{NH_3} \left(\frac{295}{T}\right)^{\Gamma_{NH_3}} \quad (\text{GHz}), \tag{15}$$

$$\zeta_j = \zeta_{H_2} P_{H_2} \left(\frac{300}{T}\right)^{Z_{H_2}} + \zeta_{He} P_{He} \left(\frac{300}{T}\right)^{Z_{He}}$$
$$+ \zeta_{NH_3} \gamma_{(0,j)} P_{NH_3} \left(\frac{295}{T}\right)^{Z_{NH_3}} \quad (\text{GHz}), \tag{16}$$

where for the inversion line j and $i = H_2$, He, and NH_3, γ_i and ζ_i are constant scale terms, and Γ_i and Z_i represent the constant temperature dependences of the broadening of each of the gases, P_i are the ideal partial pressures in bar, and $\gamma_{(0,j)}$ are the self-broadening linewidths of the inversion transitions of ammonia in MHz/Torr. The units of $\gamma_{(0,j)}$ remain in MHz/Torr and the conversion to GHz/bar is incorporated in the scale terms γ_{NH_3} and ζ_{NH_3} in Eqs. (15) and (16). The values for $\gamma_{(0,j)}$ are from the calculations of Poynter and Kakar (1975) assuming a T_0 of 295 K. For the lines with center frequencies below 7.2 GHz and $J > 16$, where J represents the total angular momentum vector for the ammonia molecule, γ_0 is expressed as

$$\gamma_0(J, K) = 25.923 \frac{K}{\sqrt{J(J+1)}} \quad (\text{MHz/Torr}), \tag{17}$$

where K is the projection of J onto the molecular axis. The $\gamma_{(0,j)}$ of all the other inversion lines which are not listed by Poynter and Kakar (1975) and whose $J < 16$ or center frequency >7.2 GHz are assigned a constant value equal to the average of the γ_0 of the lines calculated by Poynter and Kakar. The pressure shift parameter is calculated by

$$\delta_j = d \times \gamma_j \quad (\text{GHz}), \tag{18}$$

where d is an empirically derived constant. All the inversion transitions are assigned the same set of model constants (either low-pressure or high-pressure), even though each line transition behaves differently (see, e.g. Hanley et al., 2009). The equation for computing the opacity from the inversion transitions has 14 free parameters. Two sets of free-parameters were empirically derived by data fitting (Tables 4 and 5) and the appropriate set of values should be used for calculating the ammonia opacity for a given pressure. Although the pressure-switch is at 15 bars, by using the low-pressure parameters at $P \leqslant 10$ bars and the high-pressure parameters at $P > 20$ bars, and values linearly interpolated with pressure between the 10 and 20 bar pressure level, it is possible to achieve a smooth pressure transition. This recommendation of the transition region values of 10 and 20 bars is based on an empirical evaluation of the model fit near the transition region to the measured data.

The opacity from the rotational transitions is calculated using a modified Gross lineshape and is given as

$$\alpha_{rot} = \frac{0.1 D_{rot} P_{NH_3}}{k_B T} \left(\frac{1}{\pi}\right) \left(\frac{T_0}{T}\right)^{\eta+1}$$
$$\times \sum_j \left[I_j(T_0) \exp \left(\left(\frac{1}{T_0} - \frac{1}{T} \right) E_{(l,j)} \left(\frac{hc}{k_B} \right) \right) \left(\frac{v}{v_{(0,j)}} \right) \left(\frac{4 v v_{(0,j)} \Delta v_j}{\left(v_{(0,j)}^2 - v^2 \right)^2 + 4 v^2 \Delta v_j^2} \right) \right] \quad (\text{cm}^{-1}), \tag{19}$$

where for the rotational line j, $v_{(0,j)}$ is the frequency of transition, Δv_j is the linewidth parameter, and D_{rot} is an empirically derived unitless scale factor. The linewidth parameter is given as

$$\Delta v_j = c_{H_2} \Delta v_{(H_2,j)} P_{H_2} \left(\frac{300}{T}\right)^{\xi_{H_2}} + c_{He} \Delta v_{(He,j)} P_{He} \left(\frac{300}{T}\right)^{\xi_{He}}$$
$$+ c_{NH_3} \Delta v_{(NH_3,j)} P_{NH_3} \left(\frac{300}{T}\right)^{\xi_{NH_3}} \quad (\text{GHz}), \tag{20}$$

Table 4
Values of the low-pressure inversion model constants used for computing the H_2/He-broadened NH_3 absorptivity when $P \leqslant 10$ bar.

	$i = H_2$	$i = He$	$i = NH_3$
γ_i	1.7465	0.9779	0.7298
Γ_i	0.8202	1	1
ζ_i	1.2163	0.0291	0.5152
Z_i	0.8873	0.8994	2/3
d	−0.0627		
D_{inv}	0.9862		

Table 5
Values of the high-pressure inversion model constants used for computing the H_2/He-broadened NH_3 absorptivity when $P > 20$ bar.

	$i = H_2$	$i = He$	$i = NH_3$
γ_i	1.6361	0.4555	0.7298
Γ_i	0.8	0.5	1
ζ_i	1.1313	0.1	0.5152
Z_i	0.6234	0.5	2/3
d	0.2		
D_{inv}	1.3746		

where for $i = H_2$, He, and NH_3, c_i and ξ_i are the empirically derived model constants, P_i are the ideal partial pressures in bar, and $\Delta v_{(i,j)}$ are the broadening parameters in GHz/bar. The units of Δv_j should be converted from GHz to cm^{-1} before it is used in the equation for computing the opacity from the rotational lines (Eq. (19)). For the linewidths, either measured or calculated values are used (see Devaraj et al. (2011) for more details).

The empirically derived model constants for the rotational transitions were given by Devaraj et al. (2011) and are listed in Table 6.

The opacity from the v_2 roto-vibrational transitions is calculated using a modified Gross lineshape and is given as

$$\alpha_{v_2} = \frac{0.1 D_{v_2} P_{NH_3}}{k_B T} \left(\frac{1}{\pi}\right) \left(\frac{T_0}{T}\right)^{\eta+1}$$
$$\times \sum_j \left[I_j(T_0) \exp\left(\left(\left(\frac{1}{T_0} - \frac{1}{T}\right) E_{(l,j)} \left(\frac{hc}{k_B}\right)\right)\right) \left(\frac{v}{v_{(0,j)}}\right) \right.$$
$$\left. \left(\frac{4 v v_{(0,j)} \Delta v}{\left(v_{(0,j)}^2 - v^2\right)^2 + 4 v^2 \Delta v^2}\right) \right] \quad (cm^{-1}), \quad (21)$$

where, for the v_2 roto-vibrational line j, $v_{(0,j)}$ is the frequency of transition, Δv is the linewidth parameter, and D_{v_2} is an empirically derived unitless scale factor. The linewidth parameter is given by

$$\Delta v = \Delta v_{H_2} P_{H_2} \left(\frac{300}{T}\right)^{\xi_{H_2}} + \Delta v_{He} P_{He} \left(\frac{300}{T}\right)^{\xi_{He}}$$
$$+ \Delta v_{NH_3} P_{NH_3} \left(\frac{300}{T}\right)^{\xi_{NH_3}} \quad (GHz), \quad (22)$$

where for $i = H_2$, He, and NH_3, ξ_i are the empirically derived temperature coefficients, P_i are the ideal partial pressures in bars, and Δv_i are the empirically derived broadening parameters for the v_2 transitions in GHz/bar. The units of Δv should be converted from GHz to cm^{-1} before it is used in the equation for computing the opacity (Eq. (21)). The linewidths were empirically calculated for the v_2 roto-vibrational transitions (see Devaraj et al. (2011) for more details).

The empirically derived model constants for the v_2 roto-vibrational transitions were derived by Devaraj et al. (2011) and are listed in Table 7.

The values of the model constants were optimized for the JPL spectral line catalogs (Pickett et al., 1998). The spectral line catalogs are periodically updated, and the version 5 catalog updated on September 2010 must be used with this particular model. The

Table 6
Values of the model constants of the new model used for computing the H_2/He-broadened NH_3 absorptivity from the rotational transitions (Devaraj et al., 2011).

	$i = H_2$	$i = He$	$i = NH_3$
c_i	0.2984	0.75	3.1789
ξ_i	0.8730	2/3	1
D_{rot}	2.4268		

Table 7
Values of the model constants of the new model used for computing the H_2/He-broadened NH_3 absorptivity from the v_2 roto-vibrational transitions (Devaraj et al., 2011).

	$i = H_2$	$i = He$	$i = NH_3$
Δv_i (GHz/bar)	1.4	0.68	9.5
ξ_i	0.73	0.5716	1
D_{v_2}	1.1206		

frequency, line intensity, and lower state energy of the various transitions of ammonia given in the latest JPL catalogs along with the self- and hydrogen-/helium-broadening parameters for these transitions are provided online (*ammonia_inversion. dat, ammonia_rotational.dat, ammonia_rotovibrational.dat*). Software for running the model in Matlab® is also provided online (*NH3H2HeModel.m*). This model can be used to estimate the opacity of ammonia under jovian conditions in the centimeter-wavelength range at pressures up to 100 bar and temperatures in the 200 to 500 K range and in the millimeter-wavelength range at pressures up to 3 bar and temperatures in the 200 to 300 K range.

3.3. Model performance

The model performance is evaluated to estimate the goodness of fit and the conditions of the model's effectiveness. (Note: The model uses the low-pressure inversion line parameters at $P \leqslant 10$ bars, high-pressure inversion line parameters at $P > 20$ bars, and a linear interpolation of the two values between 10 and 20 bars.) The model was compared with the 1431 data points of the 1.5–27 GHz opacity of ammonia and the 250 data points of the 22–40 GHz opacity of ammonia measured by Hanley et al. (2009), 1013 data points of the 75–150 GHz opacity of ammonia measured by Devaraj et al. (2011) and the 1176 data points of the 1.5–6 GHz opacity of ammonia measured as part of this work.

The new ammonia opacity model fits 66.64% of the 1.5–6 GHz high-pressure cavity resonator measurements, 65.15% of the 75–150 GHz FPR measurements, 94.23% of the 1.5–27 GHz cavity resonator measurements, and 89.92% of the 22–40 GHz FPR measurements within 2σ uncertainty. Overall, the model fits 76.77% of the 3870 measurements in the 1.5–150 GHz range within 2σ uncertainty. Comparison of the new model performance with the models of Berge and Gulkis (1976), Spilker (1990), Joiner and Steffes (1991), Mohammed and Steffes (2003), Mohammed and Steffes (2004), Hanley et al. (2009), Hanley (2008) with rotational lines, and Devaraj et al. (2011) is listed in Table 8. Plots comparing some of the measured data to the different models are shown in Figs. 3–6. The error bars shown in the plots are the 2σ measurement uncertainties. (Note: The measurements near ~5.3 GHz and ~5.9 GHz were made with resonances that were highly asymmetric, hence the error bars are large for those measurements.).

In the implementation of the model by Joiner and Steffes (1991), there were difficulties in matching the numerical values given by the authors. Hanley et al. (2009) describe similar difficulties in reproducing the original numerical values given by Joiner and Steffes (1991). However, the numerical values estimated by Hanley et al. (2009) for the various models are consistent with the values estimated in this work (note that archival versions of the line catalog used for their model are available). The Hanley et al. (2009) model includes only the inversion transitions of ammonia and was developed using their centimeter-wavelength measurements conducted at pressures up to 12 bar. Hanley (2008) provided a modification to this model for use in the high-pressure regime by including the lowest 20 rotational transitions

Table 8
The percentage of the NH₃—He—H₂ measurement data points within 2σ uncertainty of the new model in comparison with the existing models.

NH₃ opacity model	Cavity (1.5–27 GHz)	FPR (22–40 GHz)	FPR (75–150 GHz)	High pressure (1.5–6 GHz)	Total
Berge and Gulkis (1976)	53.11	89.2	23.59	56.72	48.81
Spilker (1990)	70.23	48.4	8.69	25.6	39.15
Joiner and Steffes (1991)	82.88	84.4	19.84	60.03	59.53
Mohammed and Steffes (2003)	57.16	55.2	3.95	37.5	37.13
Mohammed and Steffes (2004)	49.13	86.4	25.07	52.55	46.28
Hanley et al. (2009)	96.09	85.2	10.46	61.73	62.5
Hanley (2008) w/ rot. lines	96.09	85.6	12.04	61.82	62.99
Devaraj et al. (2011)	95.11	94.8	66.44	35.46	69.46
This work	**94.23**	**89.92**	**65.15**	**66.64**	**76.77**
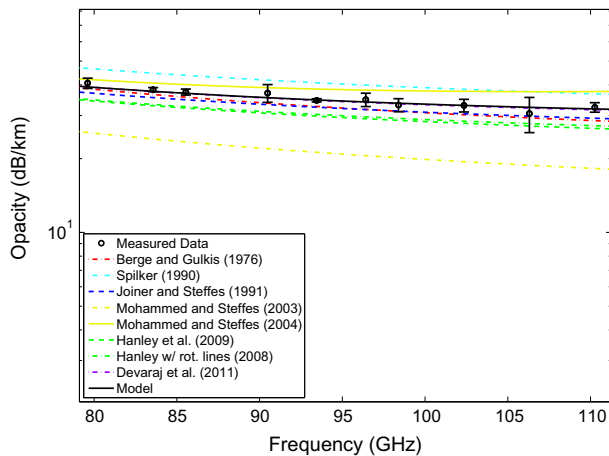
Fig. 3. Opacity data measured using the 3–4 mm-wavelength system for a mixture of NH₃ = 4%, He = 13.06%, H₂ = 82.94% at a pressure of 1.999 bar and temperature of 296.2 K compared to various models.
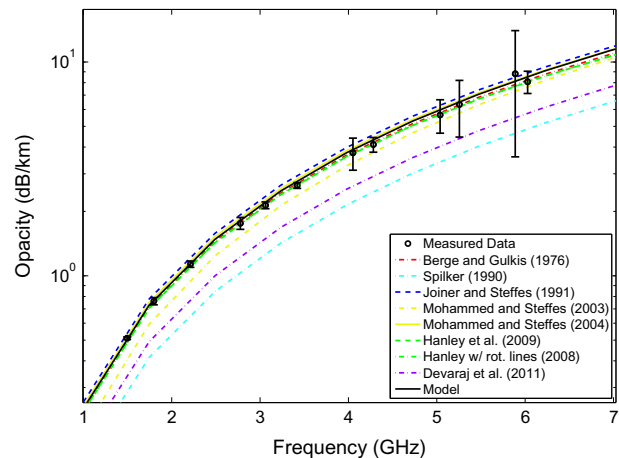
Fig. 5. Opacity data measured using the high-pressure centimeter-wavelength system for a mixture of NH₃ = 0.09%, He = 0%, H₂ = 99.91% at a pressure of 93.545 bar and temperature of 446.9 K compared to various models.
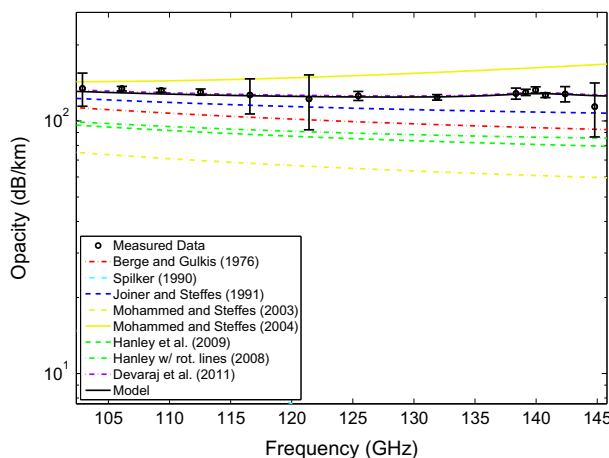
Fig. 4. Opacity data measured using the 2–3 mm-wavelength system for a mixture of NH₃ = 6.2%, He = 12.76%, H₂ = 81.04% at a pressure of 1.909 bar and temperature of 220.7 K compared to various models.
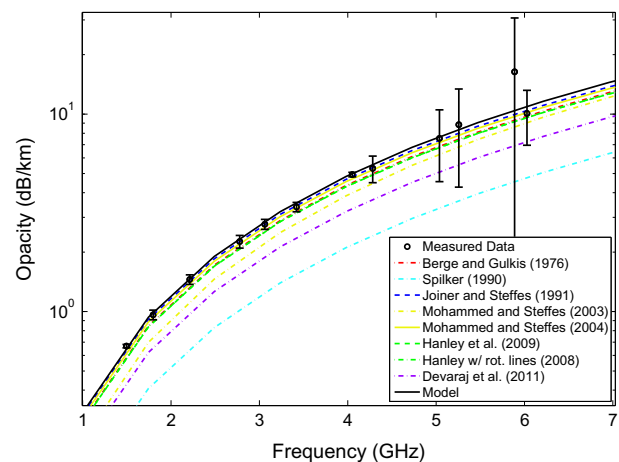
Fig. 6. Opacity data measured using the high-pressure centimeter-wavelength system for a mixture of NH₃ = 0.13%, He = 10.92%, H₂ = 88.95% at a pressure of 98.439 bar and temperature of 502.1 K compared to various models.

of ammonia in addition to the inversion transitions, and both the models are shown in the figures for comparison. The difference between the new model for ammonia opacity in an H₂/He atmosphere and that of Hanley et al. (2009) becomes more pronounced when extrapolated to higher temperatures than those measured here. For example, at a temperature of 600 K and total mixture pressure of 80 bars, our new model predicts ∼20% more opacity than that computed by the Hanley et al. (2009) model. Thus, care should be taken when extrapolating either model beyond the temperature and pressure ranges used in the experiments. Future

work will include study of how to best assure accurate extrapolation to higher temperatures.

3.4. Ultra-high-pressure extrapolation

The new consistent ammonia opacity model was developed for use under jovian conditions in the centimeter-wavelength range at pressures up to 100 bar and in the millimeter-wavelength range at pressures up to 3 bar. The new model corrects for the non-ideal

pure fluid behavior under high-pressure conditions and the high-pressure inversion model parameters were empirically derived by data fitting to a high-pressure data set. While this model can be extrapolated with reasonable certainty to slightly higher pressures, some caution must be exercised when using the model under ultra-high-pressure conditions (pressures much greater than 100 bar).

When modeling the microwave emission from a planetary atmosphere, weighting functions (or contribution functions) indicate the altitudes (pressure layers) that contribute most to the brightness temperature at a particular frequency. The weighting functions probe less deep into the atmosphere at the limb of the planet than at nadir, since the path length through the atmosphere at the limb is longer than at nadir. For example, the nadir-viewing weighting function for Jupiter show that at 1 GHz the atmospheric layers from 20 to 300 bar contribute to the brightness temperature. At even lower frequencies, the jovian atmospheric layers at hundreds of bar of pressure contribute to the brightness temperature (see e.g., Karpowicz, 2010).

Morris and Parsons (1970) made measurements of the microwave absorption of ammonia in a predominantly hydrogen or helium atmosphere at 295 K and pressures up to 700 bar. A tunable resonant cavity which was operated in the TE_{013} mode was used for these measurements and the binary mixture absorption measurements were conducted at 9.58 GHz. These measurements show a steep increase in opacity with pressure up to around 80 bar, and then the opacity increases less steeply. Morris (1971) attempts to explain this behavior as a shift from resonant to non-resonant Debye absorption along with greater frequency of collision of molecules. Berge and Gulkis (1976) developed a model that was fit to the Morris and Parsons (1970) ammonia/hydrogen data using a correction factor for hydrogen. However, this model does not include a correction factor for helium, which behaves in a similar fashion to hydrogen. Hanley (2008) attempted to fit to the Morris and Parsons (1970) data by including the lowest 20 rotational transitions of ammonia. The Berge and Gulkis (1976), Hanley (2008) with rotational lines, and the new model developed as part of this work are shown along with the Morris and Parsons (1970) measured data in Figs. 7 and 8. Since the absolute uncertainties of the Morris and Parsons (1970) ammonia measurements are not precisely known, the measurements were assumed to be accurate within ±10%. There could be some additional uncertainties in the Morris and Parsons (1970) data since they did not account for the adsorption of ammonia on the walls of their system. Additionally, the measurements were made only at one resonant frequency and that resonance might have been contaminated by other resonances. Since the original Morris and Parsons (1970) data could not be obtained by the authors, a digitizing software was used to extract the data points from the plots (Note: The software used was Plot Digitizer®). Hence, there could be additional uncertainties from the digitization process, especially at the lower pressure regions where the data points are clumped together.

Although the new model seems to be consistent with the Morris and Parsons (1970) data (the new model fits 65% of the Morris and Parsons (1970) data with the assumed 10% absolute uncertainty), some caution must be exercised when using the new model at pressures much greater than 100 bar. The new model accounts for the non-ideal behavior of pure fluids, but does not account for the non-ideal behavior of fluid mixtures. Additionally, only the inversion transitions of the new model were optimized for use under high-pressure conditions (pressures up to 100 bar). The parameters for the rotational transitions described in this work were not optimized to perform under high-pressure conditions. Finally, the assumptions underlying most lineshape theories, such as binary and elastic collisions of molecules, might become invalid under ultra-high-pressure conditions.

4. The influence of water vapor on the ammonia absorption spectrum

Water vapor is the third most abundant constituent deep in the atmosphere of Jupiter after hydrogen and helium (see, e.g. Atreya et al., 2003). Current ammonia opacity models for the jovian atmospheres, including the new model described in Section 3, account for the self-broadening of ammonia and foreign-gas-broadening due to hydrogen and helium. While the pressure-broadening effects of hydrogen and helium on ammonia are well characterized, it is critical to investigate possible pressure-broadening effects of water vapor on the ammonia absorption spectrum. Karpowicz and Steffes (2011b) made extensive measurements of the intrinsic opacity of water vapor in the 5–20 cm-wavelength range under jovian conditions and found that the self-broadening from water vapor dominates its absorption spectrum. Water vapor has a large broadening cross-section (collision diameter) and has the potential to broaden the ammonia transitions.

Prior to this investigation, there was at least one laboratory study which indicated that water vapor can efficiently broaden the 572 GHz rotational transition of ammonia (Belov et al., 1983). Hence, a measurement campaign to study the influence of water vapor on the ammonia absorption spectrum was undertaken. Laboratory measurements were conducted to study possible enhancement in the opacity of ammonia in the 5–20 cm-wavelength range due to water vapor (in addition to hydrogen and helium) under simulated jovian conditions. The laboratory measurements and the model provide new and critical information that will be used to estimate the abundance of water vapor and ammonia at Jupiter by the Juno MWR.

4.1. Ammonia–water vapor opacity measurements

Laboratory measurements of the 5–20 cm-wavelength properties of ammonia pressure-broadened by water vapor in addition to hydrogen and helium have been conducted using the high-pressure system. The measurement process involved nine sequences in the 375–500 K temperature range and a total of 838 unique measurements of the 5–20 cm-wavelength opacity of ammonia–water vapor–hydrogen–helium mixture. Certified UHP grade ammonia and argon gas cylinders from Airgas, Inc. were used for the test gas and dielectric matching measurements. A water reservoir (similar to the one used by Karpowicz and Steffes, 2011b), filled with distilled water, ACS Reagent Grade with ASTM D 1193 specifications for reagent water, type II (manufactured by Ricca Chemical Company), was connected to the pressure vessel and placed inside the oven to generate the required amount of water vapor for the experiments. The water vapor adsorption by the chamber walls is very small (see, e.g. Karpowicz, 2010) when compared to ammonia under our experimental conditions. Hence, for 8 of the 9 sequences, ammonia was added first to the system to presaturate the walls of the pressure vessel and cavity resonator and pure ammonia measurements were made. For one of the measurement sequences (#4 in Table 9), water vapor was added first followed by ammonia in order to test the impact and extent of ammonia adsorption (physical adsorption or physisorption) on the measured opacity. There was no discernible effect of the adsorption of ammonia on the measured opacity at 375 K. At higher temperatures, the physisorption potential is even less. Hence, for the measurements at 375 K or higher temperatures, physisorption of ammonia is assumed to be negligible.

Each measurement sequence first involved vacuum measurements, followed by the addition of gaseous ammonia to the evacuated chamber up to the desired pressure and pure ammonia measurements were made. Water vapor was then added to the

Table 9
Listing of all experiment sequences of the 5–20 cm-wavelength opacity measurements of the NH_3—H_2O—He—H_2 mixture.

Sequence #	Experiment dates	Temperature (K)	Maximum pressure (bar)	NH_3 pressure (bar)	H_2O pressure (bar)	He pressure (bar)
1	12/2010	452.11	97.66	0.0902	0.945	8.1835
2	12/2010	452.52	96.3	0.0462	1.0912	15.015
3	02/2011	373.85	91.99	0.0295	0.1499	5.75
4	03/2011	373.85	91.33	0.0481	0.2065	13.09
5	06/2011	373.45	91.32	0.0771	0.4248	0
6	06/2011	373.05	91.69	0.0828	0.3984	17.54
7	07/2011	449.9	91.62	0.0914	1.2	8.16
8	11/2011	501.01	89.71	0.0994	2.2866	3.628
9	12/2011	501.5	89.55	0.2018	1.8462	12.076

system up to the desired pressure, by opening the oven door and quickly opening and closing the valve on the water reservoir, and ammonia/water vapor mixture measurements were made. Since there was a possibility of water vapor condensing in the pipes exterior to the oven (which were at room temperature), the high-temperature inlet and outlet valves inside the oven were closed before water vapor was added into the pressure vessel. A coarse estimate of the water vapor pressure while adding water vapor to the system was obtained from the pressure transducer readings. This was done to ensure that the water vapor partial pressure was well below the saturation vapor pressure at the measurement temperature. For the measurement sequence #4, water vapor was added first and then ammonia was added, but a similar procedure was followed for reading the pressure. After the measurements of the water vapor/ammonia mixture were conducted, an accurate pressure reading was obtained using a "buffer method". A small amount of helium was added to the pipe section connecting the DPI 10430A gauge to the inlet valve to a pressure known to be slightly greater than that in the pressure vessel (based on the initial pressure transducer readings). Then, while monitoring the DPI 10430A gauge, the oven was quickly opened and the inlet valve to the pressure vessel was opened and the pressure quickly read before closing the valve and shutting the oven door. The pressure readings stabilized very quickly and the possibility of any water vapor entering and condensing in the pipes external to the oven was very small. Since the volume of the pipe section between the DPI 10430A gauge and the inlet valve was very small relative to the volume of the pressure vessel, which is approximately 32 l, no additional corrections were needed to account for the true pressure in the vessel prior to opening the inlet valve. After the ammonia–water vapor mixture measurements, helium and hydrogen were added and measurements made at pressures up to 100 bars. After the measurements of the test gas mixture, the pressure vessel was vented down to ambient pressure and a vacuum was drawn in the pressure vessel and a second set of vacuum measurements were conducted. After this step, dielectric matching measurements were conducted followed by a third set of vacuum measurements. Finally, three sets of straight-through measurements of signal levels were conducted to correct the transmissivity measurements of the test gases and dielectric matching gases for losses in the microwave cables and connectors. A detailed explanation of the measurement procedure is provided in Section 2.2.

Table 9 lists the measurements and the experiment dates. The pressure values provided in the table correspond to the maximum measured pressure reading of the pressure sensors.

The processed data are provided in the online Supplementary materials section (*NH3H2HeH2OMeasurements.mat*).

4.2. Ammonia–water vapor opacity model

The first step in modeling the opacity of the ammonia–water vapor–hydrogen–helium mixture is the removal of the opacity of

Table 10
Values of the H_2O model constants used for computing the H_2O-broadened NH_3 absorptivity from the inversion transitions.

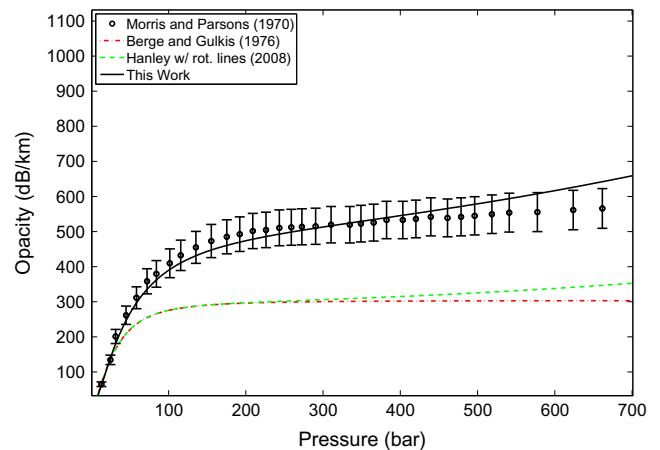|	$i = H_2O$
γ_i	4.8901
Γ_i	0.5
ζ_i	2.731
Z_i	1

Fig. 7. Opacity data by Morris and Parsons (1970) for a mixture of NH_3 = 0.9%, He = 99.1%, H_2 = 0% at a frequency of 9.58 GHz and temperature of 295 K compared to this work, Hanley (2008) with rotational lines and Berge and Gulkis (1976).

the water vapor–hydrogen–helium mixture. Karpowicz and Steffes (2011b) conducted laboratory measurements of the opacity of water vapor broadened by hydrogen and helium and developed a model for the jovian atmosphere (Karpowicz and Steffes, 2011b,a). Some water vapor model parameters provided by Karpowicz and Steffes (2011a) were modified (Note the modified parameters and their values: $C_w = 3.1 \times 10^{-7}$ km^{-1} × (mbars× GHz)$^{-2}$, $C'_w = 0$, $x_{continuum} = 12$) to improve the accuracy under the deep jovian conditions where temperatures exceed 500 K (Steffes, personal communication, December 2013). However, these modifications to the water vapor model did not affect the new ammonia–water vapor–hydrogen–helium model since the water vapor–hydrogen–helium opacity component is negligible (ammonia is the dominant contributor), and the measurements were made only at temperatures up to 500 K.

Once the intrinsic opacity of water vapor was removed, data fitting and optimization were performed in a fashion similar to that explained in Section 3.1 and a model of the opacity of ammonia pressure-broadened by water vapor was derived using the formulations given in Section 3.2. The model for the water vapor-broadened opacity of ammonia uses a modified Ben–Reuven lineshape
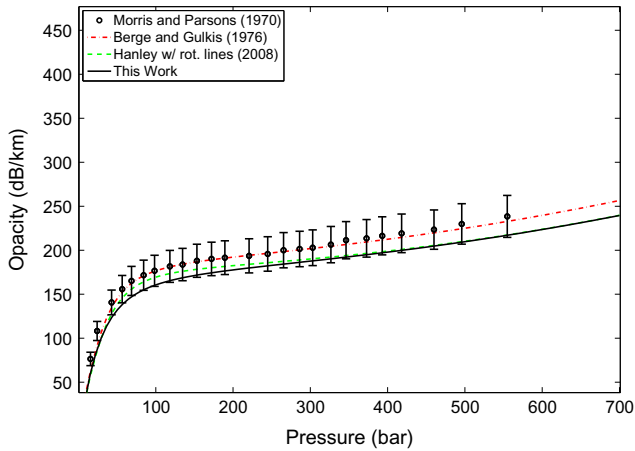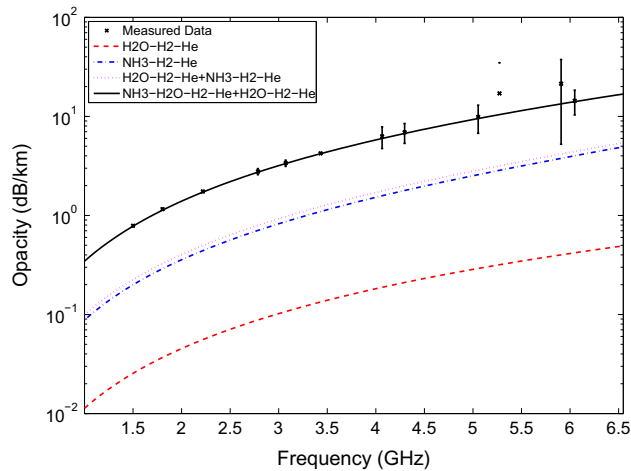
Fig. 8. Opacity data measured by Morris and Parsons (1970) for a mixture of NH_3 = 0.44%, He = 0%, H_2 = 99.56% at a frequency of 9.58 GHz and temperature of 295 K compared to this work, Hanley (2008) with rotational lines, and Berge and Gulkis (1976).

Fig. 10. Opacity data measured using the high-pressure centimeter-wavelength system for a mixture of NH_3 = 0.23%, H_2O = 2.06%, He = 13.49%, H_2 = 84.23% at a pressure of 87.351 bar and temperature of 501.2 K compared to various model. The dashed line shows the H_2O-H_2-He opacity model by Karpowicz and Steffes (2011b,a), with the additional parameter modifications provided in this paper. The dash-dotted line shows the NH_3-H_2-He opacity model described in this paper. The dotted line shows the summation of opacity contributions from the NH_3-H_2-He and H_2O-H_2-He models. The solid line shows the summation of opacity contributions from the $NH_3-H_2-He-H_2O$, that includes the effects of broadening of NH_3 by H_2O, and H_2O-H_2-He model. Inset plot shows a magnified view from 1.4 to 2.4 GHz.

Fig. 9. Opacity data measured using the high-pressure centimeter-wavelength system for a mixture of NH_3 = 9.85%, H_2O = 90.15%, He = 0%, H_2 = 0% at a pressure of 2.062 bar and temperature of 501.3 K compared to various model. The dashed line shows the H_2O-H_2-He opacity model by Karpowicz and Steffes (2011b,a), with the additional parameter modifications provided in this paper. The dash-dotted line shows the NH_3-H_2-He opacity model described in this paper. The dotted line shows the summation of opacity contributions from the NH_3-H_2-He and H_2O-H_2-He models. The solid line shows the summation of opacity contributions from the $NH_3-H_2-He-H_2O$, that includes the effects of broadening of NH_3 by H_2O, and H_2O-H_2-He model.

Fig. 11. Opacity data measured using the high-pressure centimeter-wavelength system for a mixture of NH_3 = 0.17%, H_2O = 3.93%, He = 6.23%, H_2 = 89.66% at a pressure of 57.156 bar and temperature of 501.3 K compared to various model. The dashed line shows the H_2O-H_2-He opacity model by Karpowicz and Steffes (2011b,a), with the additional parameter modifications provided in this paper. The dash-dotted line shows the NH_3-H_2-He opacity model described in this paper. The dotted line shows the summation of opacity contributions from the NH_3-H_2-He and H_2O-H_2-He models. The solid line shows the summation of opacity contributions from the $NH_3-H_2-He-H_2O$, that includes the effects of broadening of NH_3 by H_2O, and H_2O-H_2-He model. Inset plot shows a magnified view from 1.4 to 2.4 GHz.

(Ben-Reuven, 1966) for the inversion transitions. The opacity of ammonia broadened by water vapor in the centimeter-wavelength region is given by Eq. (14). The linewidth and the coupling parameter of the lines are calculated by summing the contribution from ammonia, water vapor, hydrogen, and helium.

The parameters for water vapor were empirically derived using the nine sequences of measurements, while the parameters for ammonia, hydrogen, and helium were assigned the same values derived in Section 3.2. Table 10 lists the values of the water vapor model constants of the NH_3-H_2O model. The ammonia, hydrogen and helium model constants are the same as given in Tables 4 and 5 for the low- and high-pressure conditions. Software for running the model in Matlab® is provided online (*NH3H2OH2HeModel.m*). This model can be used to estimate the opacity of ammonia in the presence of water vapor, hydrogen, and helium under jovian conditions in the centimeter-wavelength range at pressures up to 100 bar and temperatures up to 500 K.
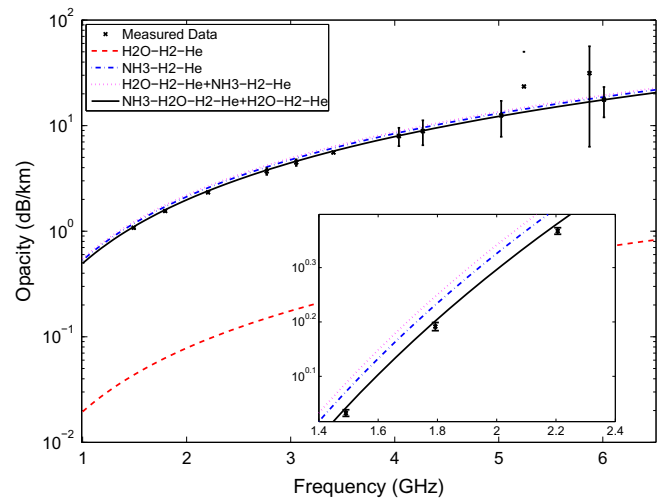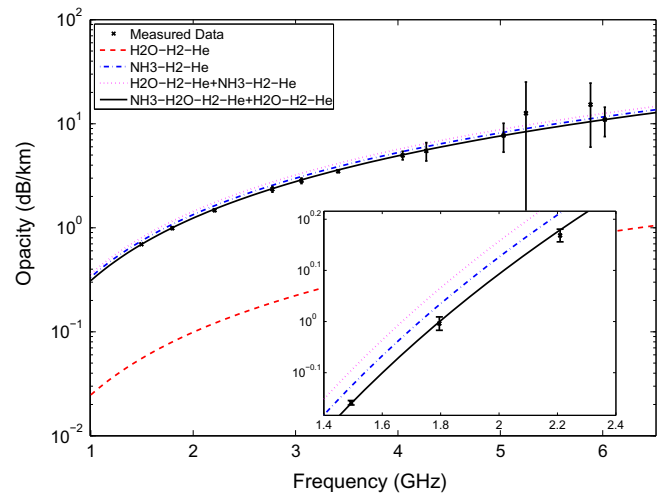
4.3. Model performance and discussion

The new model fits 63.8% of the 838 data points within 2σ uncertainty and 71.6% of the data points within 3σ uncertainty. Plots comparing some of the measured data to the relative

contribution from the two species are shown in Figs. 9–11. The error bars shown in the plots are the 2σ measurement uncertainties.

In this work, the change in the centimeter-wavelength opacity of the NH_3–H_2O mixture was considered to result from the broadening of ammonia absorption lines by water vapor. The 1–6 GHz opacity is either enhanced or reduced by the introduction of water vapor, depending on the temperature, pressure, and mixing ratio of the gases. It is possible that ammonia could broaden water vapor lines and this effect resulted in the observed change in opacity in the laboratory study. However, the latter explanation is extremely unlikely because (i) ammonia's intrinsic centimeter-wavelength opacity is roughly two orders of magnitude larger compared to water vapor, and (ii) the foreign gas broadening of water vapor (by hydrogen and helium) is 3–4 orders of magnitude smaller compared to its self-broadening (see Karpowicz and Steffes, 2011b,a), and by extension, it is reasonable to assume that the foreign gas broadening of water vapor by ammonia will also be likely much smaller than its self-broadening. Because of the combination of these two factors, we believe that the observed change in opacity in this study must be attributed to the collision broadening of ammonia absorption lines by water vapor.

5. Conclusions

Accurate laboratory measurements of the 5–20 cm-wavelength properties of ammonia in a hydrogen–helium environment under simulated tropospheric conditions of the jovian planets have been conducted. These and pre-existing laboratory measurements (Hanley et al., 2009; Devaraj et al., 2011) were utilized to develop the most accurate and consistent model to date to represent the opacity of ammonia pressure-broadened by hydrogen and helium in the centimeter-wavelength range at pressures up to 100 bars and temperatures up to 500 K and in the millimeter-wavelength range at pressures up to 3 bars and temperatures up to 300 K.

For the first time, laboratory investigation of the 5–20 cm-wavelength opacity of ammonia pressure-broadened by water vapor in addition to hydrogen and helium was conducted and a model for the centimeter-wavelength opacity of ammonia pressure-broadened by water vapor, hydrogen and helium has been developed. The measurements and the model demonstrated that water vapor, because of its large broadening cross-section, can efficiently broaden the ammonia inversion transitions and alter the total opacity contribution from ammonia. In the jovian atmospheres, depending on the concentration of water vapor, it can have a measurable effect on the ammonia opacity. Hence, foreign-gas broadening of ammonia due to minor species such as water vapor should be taken into account for accurate modeling and interpretation of the jovian emission spectrum. The influence of methane on the ammonia absorption spectrum has been studied recently at Georgia Tech. The results of this study will be published in a future article.

The ammonia–hydrogen–helium model and the ammonia–water vapor–hydrogen–helium model can be used to calculate the opacity of ammonia under jovian conditions at pressures up to 100 bars and temperatures up to 500 K. The new measurements and the model will aid retrievals of the atmospheric abundance of water vapor, ammonia, and other constituents at Jupiter from the Juno MWR measurements.

Acknowledgments

Appendix A. Supplementary data

Supplementary data associated with this article can be found, in the online version, at http://dx.doi.org/10.1016/j.icarus.2014.06.017.

References

Atreya, S., Mahaffyy, P., Niemann, H., Wong, M., Owen, T., 2003. Composition and origin of the atmosphere of Jupiter – An update, and implications for the extrasolar giant planets. Planet. Space Sci. 51, 105–112.

Belov, S.P., Krupnov, A.F., Markov, V.N., Mel'nikov, A.A., Skvortsov, V.A., Tret'yakov, M.Y., 1983. Study of microwave pressure lineshifts: Dynamic and isotopic dependences. J. Mol. Spectrosc. 101, 258–270.

Ben-Reuven, A., 1966. Impact broadening of microwave spectra. Phys. Rev. 145, 7–22.

Berge, G.L., Gulkis, S., 1976. Earth-based radio observations of Jupiter: Millimeter to meter wavelengths. In: Gehrels, T. (Ed.), Jupiter: Studies of the Interior, Atmosphere, Magnetosphere, and Satellites. Univ. of Arizona Press, Tuscon, AZ, pp. 621–692.

Bleaney, B., Loubser, J.H.N., 1950. The inversion spectra of NH_3, CH_3C1 and CH_3Br at high pressures. Proc. Phys. Soc., Sect. A. 63, 483–493.

Bleaney, B., Penrose, R.P., 1947. The inversion spectrum of ammonia at centimetre wavelengths. Proc. R. Soc. A189, 358–371.

de Pater, I., Lissauer, J.J., 2001. Planetary Sciences. Cambridge University Press, Cambridge, UK.

de Pater, I., Mitchell, D., 1993. Radio observations of the planets: The importance of laboratory measurements. J. Geophys. Res. 98, 5471–5490.

de Pater, I., DeBoer, D., Marley, M., Freedman, R., Young, R., 2005. Retrieval of water in Jupiter's deep atmosphere using microwave spectra of its brightness temperature. Icarus 173, 425–438.

DeBoer, D.R., Steffes, P.G., 1994. Laboratory measurements of the microwave properties of H_2S under simulated jovian conditions with an application to Neptune. Icarus 109, 352–366.

DeBoer, D.R., Steffes, P.G., 1996. Estimates of the tropospheric vertical structure of Neptune based on microwave radiative transfer studies. Icarus 123, 323–335.

Devaraj, K., 2011. The Centimeter- and Millimeter-wavelength Ammonia Absorption Spectra Under Jovian Conditions. PhD thesis, Georgia Institute of Technology, Atlanta, GA.

Devaraj, K., Steffes, P.G., Karpowicz, B.M., 2011. Reconciling the centimeter- and millimeter-wavelength ammonia absorption spectra under jovian conditions: Extensive millimeter-wavelength measurements and a consistent model. Icarus 212, 224–235.

Gross, E.P., 1955. Shape of collision-broadened spectral lines. Phys. Rev. 97, 395–403.

Hanley, T.R., 2008. The Microwave Opacity of Ammonia and Water Vapor: Application to Remote Sensing of the Atmosphere of Jupiter. PhD dissertation, Georgia Institute of Technology, Atlanta, GA.

Hanley, T.R., Steffes, P.G., 2007. A high-sensitivity laboratory system for measuring the microwave properties of gases under simulated conditions for planetary atmospheres. Radio Sci., 42, RS6010.

Hanley, T.R., Steffes, P.G., Karpowicz, B.M., 2009. A new model of the hydrogen and helium-broadened microwave opacity of ammonia based on extensive laboratory measurements. Icarus 202, 316–335.

Janssen, M., 1993. Atmospheric Remote Sensing by Microwave Radiometry. Wiley-Interscience Publication, Wiley, URL <http://books.google.com/books?id=SVsRAQAAIAAJ>.

Joiner, J., Steffes, P.G., 1991. Modeling of Jupiter's millimeter wave emission utilizing laboratory measurements of ammonia (NH_3) opacity. J. Geophys. Res. 96, 17,463–17,470.

Karpowicz, B.M., 2010. In Search of Water Vapor on Jupiter: Laboratory Measurements of the Microwave Properties of Water Vapor and Simulations of Jupiter's Microwave Emission in Support of the Juno Mission. PhD dissertation, Georgia Institute of Technology, Atlanta, GA.

Karpowicz, B.M., Steffes, P.G., 2011a. Corrigendum to In search of water vapor on Jupiter: Laboratory measurements of the microwave properties of water vapor under simulated jovian conditions. Icarus 214 (2), 783, URL <http://www.sciencedirect.com/science/article/pii/S0019103511002119>.

Karpowicz, B.M., Steffes, P.G., 2011b. In search of water vapor on Jupiter: Laboratory measurements of the microwave properties of water vapor under simulated jovian conditions. Icarus 212, 210–223.

Karpowicz, B.M., Steffes, P.G., 2013. Investigating the H_2–He–H_2O–CH_4 equation of state in the deep troposphere of Jupiter. Icarus 223, 277–297.

Lemmon, E.W., Huber, M.L., McLinden, M.O., 2007. NIST Standard Reference Database 23: Reference Fluid Thermodynamic and Transport Properties-REFPROP, Standard Reference Data Program Version 8.0. National Institute of Standards and Technology, Gaithersburg.

Levenberg, K., 1944. A method for the solution of certain nonlinear problems in least squares. Quart. Appl. Math. 2, 164–168.

Marquardt, D., 1963. An algorithm for least-squares estimation of nonlinear parameters. SIAM J. Appl. Math. 11, 431–441.

Matousek, S., 2005. The Juno New Frontiers Mission. Tech. Rep. IAC-05-A3.2.A.04, California Institute of Technology.

Mohammed, P.N., Steffes, P.G., 2003. Laboratory measurements of the Ka-band (7.5 to 9.2 mm) opacity of phosphine (PH_3) and ammonia (NH_3) under simulated conditions for the Cassini-Saturn encounter. Icarus 166, 423–435.

Mohammed, P.N., Steffes, P.G., 2004. Laboratory measurements of the W band (3.2 mm) properties of phosphine (PH_3) and ammonia (NH_3) under simulated conditions for the outer planets. J. Geophys. Res., 109, E07S13.

Morris, E.C., 1971. Microwave absorption by gas mixtures at pressures upto several hundred bars. II. Discussion of results. Aust. J. Phys. 24, 157–175.

Morris, E.C., Parsons, R.W., 1970. Microwave absorption by gas mixtures at pressures upto several hundred bars. I. Experimental technique and results. Aust. J. Phys. 23, 335–349.

Pickett, H.M., Poynter, R.L., Cohen, E.A., Delitsky, M.L., Pearson, J.C., Müller, H.S.P., 1998. Submillimeter, millimeter, and microwave spectral line catalog. J. Quant. Spectrosc. Radiat. Transfer 60, 883–890.

Pingree, P., et al., 2008. Microwave radiometers from 0.6 to 22 GHz for Juno, a polar orbiter around Jupiter. Proc. IEEE Aero. Conf. 50, 337–348.

Poynter, R.L., Kakar, R.K., 1975. The microwave frequencies, line parameters, and spectral constants for 14NH_3. Astrophys. J. Suppl. Ser. 29, 87–96.

Span, R., 2000. Multiparameter Equations of State. Springer, New York.

Spilker, T.R., 1990. Laboratory Measurements of the Microwave Absorptivity and Refractivity Spectra of Gas Mixtures Applicable to Giant Planet Atmospheres. PhD dissertation, Stanford University, CA.

Steffes, P.G., Jenkins, J.M., 1987. Laboratory measurements of the microwave opacity of gaseous ammonia (NH_3) under simulated conditions for the jovian atmosphere. Icarus 72, 35–47.

Townes, C.H., Schawlow, A.L., 1955. Microwave Spectroscopy. McGraw-Hill, New York.

Yu, S., Drouin, B.J., Pearson, J.C., 2010a. Species tag: 17002 Version 5. URL <http://spec.jpl.nasa.gov/ftp/pub/catalog/doc/d017002.pdf>.

Yu, S., Drouin, B.J., Pearson, J.C., 2010b. Species tag: 17004 Version 5. URL <http://spec.jpl.nasa.gov/ftp/pub/catalog/doc/d017004.pdf>.

Yu, S. et al., 2010c. Submillimeter-wave and far-infrared spectroscopy of high-J transitions of the ground and $v_2 = 1$ states of ammonia. J. Chem. Phys. 133. http://dx.doi.org/10.1063/1.3499911,174317.